Hindawi Publishing Corporation
International Journal of Photoenergy
Volume 2012, Article ID 385185, 6 pages
doi:10.1155/2012/385185

Research Article

Properties of $Cu(In,Ga)Se_2$ Thin Films and Solar Cells Deposited by Hybrid Process

S. Marsillac,[1] H. Khatri,[2] K. Aryal,[1] and R.W. Collins[2]

[1] *Department of Electrical and Computer Engineering, Old Dominion University, Norfolk, VA 23529, USA*
[2] *Wright Center for Photovoltaics Innovation and Commercialization, University of Toledo, Toledo, OH 43606, USA*

Correspondence should be addressed to S. Marsillac, smarsill@odu.edu

Received 16 December 2011; Accepted 6 February 2012

Academic Editor: Peter Rupnowski

$Cu(In,Ga)Se_2$ solar cells were fabricated using a hybrid cosputtering/evaporation process, and efficiencies as high as 12.4% were achieved. The films were characterized by energy-dispersive X-ray spectroscopy, glancing incidence X-ray diffraction, scanning electron microscopy, auger electron spectroscopy, and transmittance and reflectance spectroscopy, and their properties were compared to the ones of films deposited by coevaporation. Even though the films were relatively similar, the ones deposited by the hybrid process tend to have smaller grains with a slightly preferred orientation along the (112) axis and a rougher surface. Both types of films have uniform composition through the depth. Characterization of these films by variable angle of incidence spectroscopic ellipsometry allowed for the calculation of the position of the critical points, via calculation of the second derivative of the dielectric function and fit with critical points parabolic band oscillators. The solar cells were then characterized by current-voltage and quantum efficiency measurements. An analysis of the diode parameters indicates that the cells are mostly limited by a low fill factor, associated mostly with a high diode quality factor ($A - 1.8$) and high series resistance ($R_s \sim 1.1\,\Omega\text{-cm}^2$) .

1. Introduction

Many technology options exist nowadays to harvest the power of the sun, a sustainable energy source, and generate electricity directly from this source via the photovoltaic effect. Among them, $Cu(In,Ga)Se_2$ has gained significant momentum as a possible high-efficiency and low-cost thin film solar cell material. Results for high-performance $Cu(In,Ga)Se_2$ solar cells have been reported with absorber material prepared either by multisource coevaporation of the elements (Cu, In, Ga, and Se) at temperatures between 550–600°C or by selenization of Cu, In, and Ga films in the presence of H_2Se gas [1–7]. These techniques are currently implemented in companies such as Wurth Solar, Global Solar, or Solar Frontier. The objective of this work is to fabricate device quality $Cu(In,Ga)Se_2$ solar cells using a process that may have greater potential for large-scale production. For the production of this thin film solar cell technology, the implementation of an easily scalable deposition process is effectively as important as the achievement of high efficiencies. One means to accomplish this goal is by introduction of a hybrid process for the deposition of the $Cu(In,Ga)Se_2$ layer using both cosputtering of the metals and evaporation of the selenium. To the best of our knowledge, device fabrication using a similar hybrid process has not been actively pursued since 1995, having achieved an efficiency near 10% on a small area device [8]. In this study, we will present results on the hybrid deposition and characterization of $Cu(In,Ga)Se_2$ thin films and solar cells and will compare these results with those from solar cells in which the $Cu(In,Ga)Se_2$ is purely coevaporated.

2. Experimental

$Cu(In,Ga)Se_2$ thin films were deposited onto molybdenum (Mo) coated soda-lime glass by a hybrid process using dc magnetron cosputtering of elemental copper (Cu), indium (In), and copper-gallium alloy (Cu-Ga: 75–25 at. %) targets along with simultaneous evaporation of selenium (Se). This is a modification of the previous process used for these films [8] with the addition of the copper source, allowing for greater flexibility in the process. Film depositions were

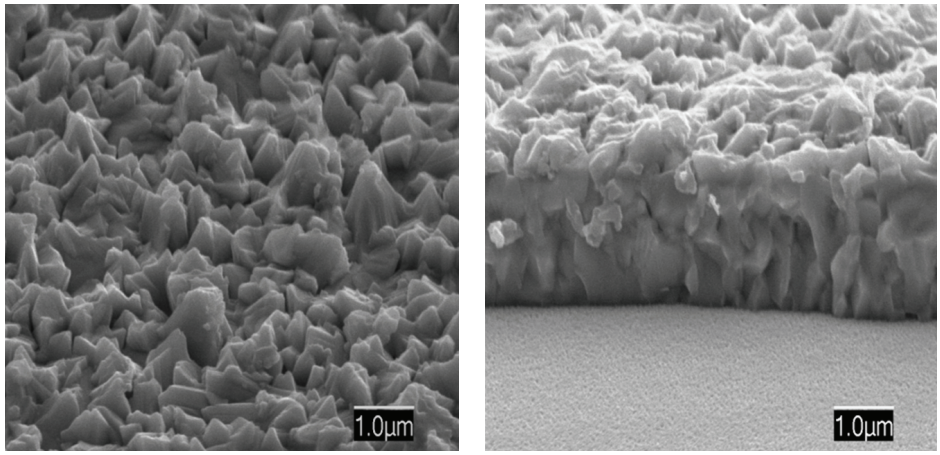

(a) (b)

Figure 1: Surface (a) and cross-sectional (b) scanning electron microscopy (SEM) images of $Cu(In,Ga)Se_2$ films deposited by a hybrid process.

performed at an Ar pressure of 2 mTorr with constant rates for the metal fluxes and the selenium. The $Cu(In,Ga)Se_2$ film thicknesses ranged from 2 μm for the devices down to 60 nm for specialized optical analysis. The substrate temperature was set at 550°C. Good uniformity of the films' elemental composition (~2%) and its thickness (~5%) were both obtained by rotating the substrate holder (15 rev/min). Coevaporated $Cu(In,Ga)Se_2$ films were also deposited and characterized for this study using a process described elsewhere [9].

3. Results and Discussions

The elemental composition of the films was determined by energy dispersive X-ray spectroscopy (EDS). The ratios x ≡ Ga/(In +Ga) and y ≡ Cu/(In +Ga) were found to be 0.30 and 0.93, respectively, which results in an energy band-gap, E_g, of 1.16 eV. Figure 1 shows representative surface and cross-sectional images of the 2 μm thick $Cu(In,Ga)Se_2$ film by scanning electron microscopy (SEM). The images reveal that the hybrid-sputtered $Cu(In,Ga)Se_2$ films have well-defined columnar grains with an average grain size of ~300 nm. This size is smaller than that of the films grown by the coevaporation process for the same composition.

Glancing incidence X-ray diffraction (GIXRD) measurements were performed using CuKα-radiation (λ = 0.15418 nm) with a 0.01° step size and various incidence angles ranging from 0.5° to 10°. The $Cu(In,Ga)Se_2$ films form a single-phase tetragonal crystal structure. The relative crystal orientations of the films prepared by hybrid sputtering and by coevaporation were 0.8 and 0.6, respectively, as measured by the ratio of the area under the (112) and (220)/(204) peaks. This indicates a slightly preferred orientation along the (112) axis for the hybrid-deposited films versus a random orientation for the coevaporated films. The average crystallite size, as determined by the full width at half maximum using Scherrer formula [10], was 393 nm for the hybrid films, which is consistent with the SEM images. The coevaporated films show a larger grain size, above the sensitivity range of this method. Little variation of the peaks was observed as a function of incidence angle indicating a constant compositional profile with depth into the film. This was corroborated by Auger electron spectroscopy measurements, which did not show any variation in composition as a function of depth.

The dielectric functions ($\varepsilon_1, \varepsilon_2$) of $Cu(In,Ga)Se_2$ thin films (60 nm) deposited by the hybrid and coevaporation processes were obtained by variable angle of incidence spectroscopic ellipsometry over the photon energy range from 0.74 eV to 6.6 eV. Thinner films were selected due to their relatively smooth surfaces, which provide higher accuracy results. It should be emphasized, however, that the thinner films may exhibit a smaller grain size and a different preferential grain orientation, factors that may lead to a difference in these dielectric functions relative to those of the thick films used in solar cells.

Given the uniaxial optical nature of the tetragonal chalcopyrite crystal structure, small differences exist between the ordinary and extraordinary dielectric function components of the single crystal. For (112) oriented films as well as for random orientation, the dielectric function is a weighted superposition of ordinary and extraordinary components [11]. In this study, an isotropic model for the dielectric function of the films was assumed. The optical model consists of (i) the soda-lime glass substrate (SLG); (ii) an interface roughness or modulation layer (thickness: d_i) between the SLG and $Cu(In,Ga)Se_2$, whose dielectric function is determined from an effective medium theory as a 0.5/0.5 volume fraction mixture of glass and the overlying bulk layer $Cu(In,Ga)Se_2$; (iii) the bulk layer $Cu(In,Ga)Se_2$ (thickness: d_b); (iv) a surface roughness layer (thickness: d_s), whose dielectric function is determined similarly to that of the interface—now as a 0.5/0.5 volume fraction mixture of the bulk layer material and void.

Figure 2 shows the results of an analysis of *ex-situ* spectroscopic ellipsometry data for the $Cu(In,Ga)Se_2$ films,

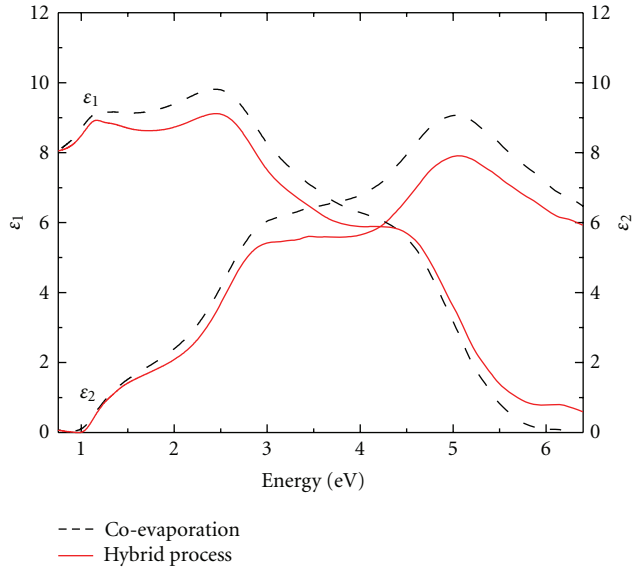

FIGURE 2: Optical dielectric functions for $Cu(In,Ga)Se_2$ films deposited by the hybrid process (solid line) and coevaporation process (dotted line).

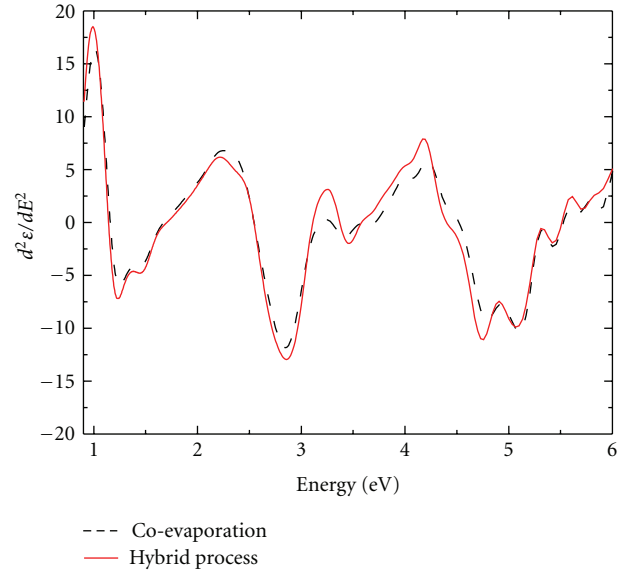

FIGURE 3: Second derivatives of the imaginary parts of the dielectric functions (ε_2) of 60 nm $Cu(In,Ga)Se_2$ films obtained by hybrid (solid line) and coevaporation processes (dotted line).

applying the optical model of the previous paragraph along with exact inversion. The photon-energy-independent parameters are obtained via the artifact-minimization/semiconductor criterion. In this procedure, bulk, surface, and interface layer thicknesses are chosen to ensure that the imaginary part of the dielectric function ε_2 is constantly below the absorption onset and as close as possible to zero. Such analysis led to the following numerical values for the films by the hybrid process: bulk layer thickness $d_b = 60 \pm 0.6$ nm; surface roughness layer thickness $d_s = 8 \pm 0.3$ nm; interface layer thickness $d_i = 1.4 \pm 0.2$ nm. Similarly, the corresponding parameters for the coevaporated $Cu(In,Ga)Se_2$ film were $d_b = 61 \pm 0.5$ nm, $d_s = 6 \pm 0.6$ nm, and an interface layer thickness $d_i = 1.7 \pm 0.3$ nm. The surface roughness was also measured by noncontact mode atomic force microscopy (AFM) and correlated well with the values obtained by ellipsometry analysis. Values of 6 nm and 4 nm were obtained for the hybrid and coevaporation processes, respectively, indicating a slightly rougher surface for the hybrid process as mentioned earlier.

The dielectric functions (ε_1, ε_2) for the hybrid deposited and coevaporated films are obtained as shown in Figure 2 simultaneously with the identification of the correct (d_b, d_s, d_i) by the artifact-minimization/semiconductor criterion.

The observed features in (ε_1, ε_2) are associated with interband transitions that appear at the van Hove singularities or critical points (CPs) of the joint density of states. These features were fitted assuming parabolic bands (PBs), yielding CP-PB oscillators each given by

$$\varepsilon_j(\hbar\omega) = \left[A_j \exp\left(i\phi_j\right)\right]\left(\hbar\omega - E_j + i\Gamma_j\right)_j^n, \tag{1a}$$

$$\varepsilon_j(\hbar\omega) = \left[A_j \exp\left(i\phi_j\right)\right]\ln\left(\hbar\omega - E_j + i\Gamma_j\right), \tag{1b}$$

where A_j is the amplitude, E_j is the energy, Γ_j is the broadening, and ϕ_j is the phase, all for the jth critical point. The exponent n_j is -1, $-1/2$, 0 (i.e., the "ln" function in (1b)), or +1/2 for excitonic, 1-dimensional, 2-dimensional, or 3-dimensional CPs, respectively. Here the fundamental transitions were fitted with excitonic CPs, and the higher transition points were fitted with 2-dimensional CPs. Because some CPs were not easily resolved, the second derivatives of the dielectric functions were used in fitting the CP-PB oscillators, as follows [12–15]:

$$\frac{d^2\varepsilon}{dE^2} = \left[A_j' \exp\left(i\phi_j\right)\right]\left(E - E_j + i\Gamma_j\right)_j^{n-2}, \tag{2}$$

where $E = \hbar\omega$ is the photon energy. The remaining four parameters for each CP were obtained in fits to the second derivatives of the dielectric functions obtained as described elsewhere [13]. The polynomial order and number of grouped data points used in this differentiation procedure were chosen to smooth the second-order derivatives without excessive line-shape distortion. The derivatives of the imaginary parts (ε_2) of the dielectric functions are shown in Figure 3 for both types of films. A sum of up to twelve resonances of the form of (2) was used to simulate the convolved ordinary and extraordinary dielectric functions of the polycrystalline $Cu(In,Ga)Se_2$ thin films.

The second derivatives of the imaginary parts dielectric functions of $Cu(In,Ga)Se_2$ thin films deposited by both processes in Figure 3 show similar positions for the CP energies. The following electronic transition assignments for the hybrid process are based on a comparison with those of a single crystal [15]. The E_0 transition energies are as follows: $E_0(A) = 1.15$ eV, $E_0(B) = 1.23$ eV, $E_0(C) = 1.46$ eV. The value for $E_0(A)$, the fundamental energy band-gap, when applied to extract composition, yields results in excellent agreement

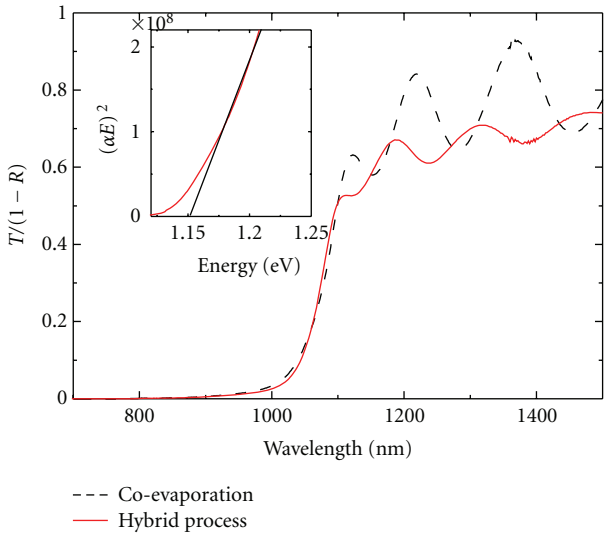

Figure 4: Room temperature $T/(1-R)$ spectra of 2 μm thick Cu(In,Ga)Se_2 films; the inset is a plot of $(\alpha E)^2$ versus E for the hybrid deposited sample.

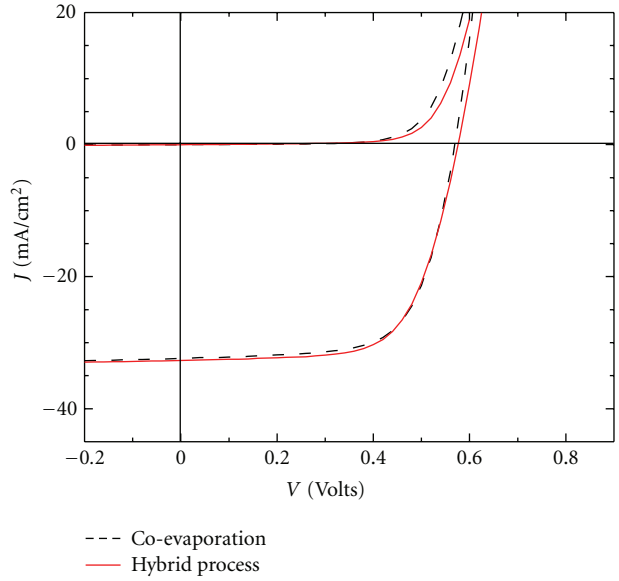

Figure 5: Current density-Voltage (J-V) characteristics of Cu(In,Ga)Se_2 solar cells deposited by hybrid and coevaporation processes.

with those obtained by EDS and XRD measurements. Three high energy transitions, namely, E_3–E_5 were also identified; however, assignments to specific electronic transitions in the band-structure are not yet possible. The following describes the higher energy CPs obtained in this analysis: $E_1(A)$ = 2.95 eV, $E(X\Gamma)$ = 3.31 eV, $E_1(B)$ = 3.75 eV, $E(\Delta X)$ = 4.19 eV, $E'(\Gamma X)$ = 4.23 eV, $E_2(A)$ = 4.61 eV, $E_2(B)$ = 4.86 eV, E_3 = 5.14 eV, E_4 = 5.47 eV, and E_5 = 5.94 eV. The CPs are not only directly useful for determining the band gap, which is a critical parameter for the solar cell, but also potentially useful for distinguishing between two materials with different properties that may lead to different device performance parameters. For example, the broadening parameters can provide information on the grain size.

Since Cu(In,Ga)Se_2 is a direct gap semiconductor [16], the absorption coefficient α is predicted to follow the well-known relationship $(\alpha n E)^2 = A(E - E_g)$ for $E > E_g$, where E_g is the energy band-gap and n is the refractive index. Thus, to determine the band-gap, it is usual to measure α by transmittance and reflectance (T and R) spectroscopy and then to extrapolate linear plots of $(\alpha E)^2$ versus E to zero ordinate as shown in Figure 4. This is based on the assumption that n is weakly varying with respect to energy in the range of interest. As one can see, a value of E_g = 1.16 eV was obtained for the hybrid process, consistent with the critical point energy $E_0(A)$ obtained by analysis of the dielectric function. It is also interesting to note that the interference fringe amplitude for the coevaporated film is larger, indicating a smoother surface since the film thicknesses are essentially identical.

After the films were fully characterized using the methods described, solar cells were fabricated by the two processes. This requires depositing a thin n-CdS buffer layer (~50 nm) by chemical bath deposition (CBD) and two rf magnetron-sputtered window layers that consist of a highly resistive intrinsic zinc oxide (80 nm) and a conductive and transparent indium tin oxide (180 nm). To enhance current collection, the device was completed by the thermal evaporation of Ni/Al/Ni metal grids with thicknesses of 50 nm/2 μm/50 nm. Finally, a MgF_2 antireflection coating (130 nm) was deposited by thermal evaporation. The cell area of 0.5 cm^2 was defined by mechanical scribing.

The current density-voltage (J-V) measurements of the completed devices were performed under standard test conditions (AM 1.5 global spectrum at 25°C, 100 mW/cm^2). We observed uniform cell performance, with efficiencies greater than 11%, for 1 inch by 3 inch substrates incorporating 26 small area devices (0.50 cm^2). The best cell exhibited an efficiency of 12.4%, with the following critical cell parameters: open circuit voltage V_{oc} = 576 mV, short-circuit current density J_{sc} = 32.7 mA/cm^2 and fill factor FF = 66%. In Figure 5, the J-V curve for the best device by the hybrid process is compared with a similar device deposited by single-stage coevaporation.

Quantum efficiency (QE) measurements were also performed on the best hybrid cell and on a coevaporated cell (Figure 6). The two QE cells are nearly indistinguishable in agreement with their similar current and band gap. The calculation of the current from the QE curve by integrating the data over the entire spectrum leads to value identical to the ones obtained via the J-V curves and confirmed the proper calibration of our system and correct area of the cells. The QE onset in the near infrared (~1070 nm) is consistent with the energy band-gap obtained from the EDS, XRD, and optical measurements.

In the near-infrared region >900 nm, the slight drop in QE for the hybrid cell may be explained by a higher recombination rate for electrons generated by photons absorbed

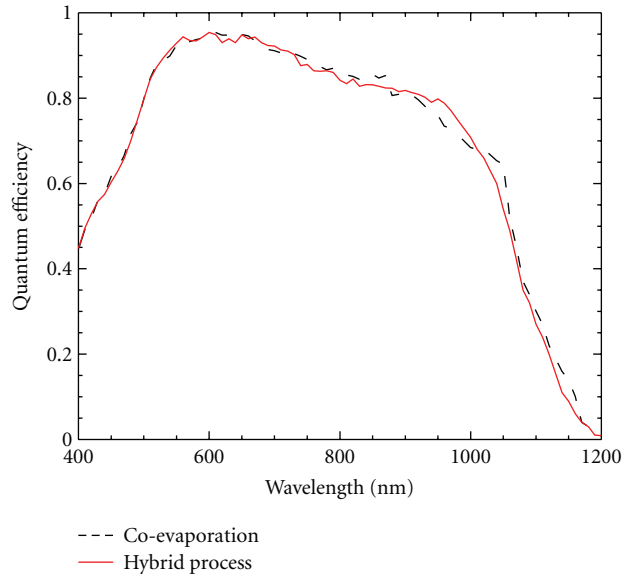

Figure 6: Normalized quantum efficiency (*QE*) characteristics for $Cu(In,Ga)Se_2$ solar cells deposited by hybrid and coevaporation processes.

deep within the $Cu(In,Ga)Se_2$ layer (i.e., towards the Mo back electrode) and/or by photon absorption by a larger concentration of free carriers in the ITO of the hybrid cell.

The *J-V* data were then analyzed using the standard diode equation considering that the forward diode current is limited by Shockley-Read-Hall (SRH) recombination through the states within the Space Charge Region (SCR) of the $Cu(In,Ga)Se_2$. The diode equation is given by

$$J = J_0 \exp\left(\frac{q(V - R_s J)}{AkT}\right) - J_0 - J_L + GV, \tag{3}$$

where J_0 is the forward current, A the diode quality factor, R_s the series resistance, J_L the light generated current, and G the shunt conductance. The shunt conductance, calculated from the *J-V* characteristics in the dark was found to be small for both types of devices and is, therefore, neglected in our device analysis. Differentiation of (3) with $J_L = J_{sc}$ leads to

$$\frac{dV}{dJ} = R_s + \frac{AkT}{q}(J + J_{sc})^{-1}. \tag{4}$$

For the $Cu(In,Ga)Se_2$ films deposited by hybrid sputtering, we found that $R_s \sim 1.1\,\Omega\text{-cm}^2$ and $A \sim 1.8$, whereas for the films deposited by coevaporation, $R_s \sim 0.8\,\Omega\text{-cm}^2$ and $A \sim 1.6$. These data were derived from the slope and intercept, respectively, in a linear fit to dV/dJ plotted versus $(J + J_{sc})^{-1}$. Classically, the value of A is between 1 and 2. The higher value for the diode quality factor in the case of the hybrid process appears to indicate that the main recombination mechanism is more closely related to interface recombination than to space charge region recombination. The higher value of the series resistance for the hybrid process might also be correlated to its higher surface roughness. Further characterization of the devices, as a function of temperature, for example, would be necessary to investigate further this difference.

4. Conclusion

The fabrication and characterization of $Cu(In,Ga)Se_2$ thin films deposited by a hybrid process were performed, and solar cells with efficiencies as high as 12.4% were achieved. Chemical, structural, and optical characterization indicates that the properties of films deposited by the hybrid process are very close to those deposited by a standard coevaporation process. The primary differences include a smaller grain size and thicker surface roughness for the hybrid process. The device performance characteristics are also found to be very similar in this study. Two aspects of this study should be emphasized, however. First, we are currently achieving higher efficiencies by coevaporation using a 3-step process; our modified hybrid process will allow us to do similar multistep deposition in the future. Second, the hybrid device performance is primarily limited by a low fill factor, which may be due to parameters other than those associated with $Cu(In,Ga)Se_2$ material limitations. As a result, further improvement in the hybrid process is expected, and the performance achieved here is not the ultimate limit of the optimization process. Overall, this new hybrid co-sputtering/evaporation process has demonstrated the capability of fabricating devices with reasonable efficiency and high uniformity and, therefore, is a promising process for potential scale up in the future.

References

[1] P. Jackson, D. Hariskos, E. Lotter et al., "New world record efficiency for $Cu(In,Ga)Se_2$ thin-film solar cells beyond 20%," *Progress in Photovoltaics*, vol. 19, no. 7, pp. 894–897, 2011.

[2] I. Repins, M. A. Contreras, B. Egaas et al., "19.9% efficient $ZnO/CdS/CuInGaSe_2$ solar cell with 81.2% fill factor," *Progress in Photovoltaics*, vol. 16, no. 3, pp. 235–239, 2008.

[3] S. Marsillac, P. D. Paulson, M. W. Haimbodi et al., "High-efficiency solar cells based on $Cu(InAl)Se_2$ thin films," *Applied Physics Letters*, vol. 81, no. 7, pp. 1350–1352, 2002.

[4] L. Eldada, "Thin film CIGS photovoltaic modules: monolithic integration and advanced packaging for high performance, high reliability and low cost," in *Proceedings of The International Society for Optical Engineering*, vol. 7942 of *Proceedings of SPIE*, 2011.

[5] A. Meeder, P. Schmidt-Weber, U. Hornauer et al., "High voltage $Cu(In,Ga)S_2$ solar modules," *Thin Solid Films*, vol. 519, no. 21, pp. 7534–7536, 2011.

[6] D. Schmid, I. Koetschau, A. Kampmann et al., "Centrotherm's high end CIGS thin film turnkey solution," in *Proceedings of the International Society for Optical Engineering*, Wuhan, China, August 2009.

[7] Y. Chiba, S. Kijima, H. Sugimoto et al., "Achievement of 16% milestone with 30 cm × 30 cm-sized CIS-based thin-film submodules," in *Proceedings of the IEEE Photovoltaic Specialists Conference*, pp. 164–168, Honolulu, Hawaii, USA, June 2010.

[8] L. C. Yang and A. Rockett, "Cu-Mo contacts to $CuInSe_2$ for improved adhesion in photovoltaic devices," *Journal of Applied Physics*, vol. 75, no. 2, pp. 1185–1189, 1994.

[9] P. D. Paulson, M. W. Haimbodi, S. Marsillac, W. N. Shafarman, and R. W. Birkmire, "$CuIn_{1-x}Al_xSe_2$ thin films and solar cells,"

Journal of Applied Physics, vol. 91, no. 12, pp. 10153–10156, 2002.

[10] N. Kasai and M. Kakudo, *X-Ray Diffraction by Macromolecules*, vol. 80 of *Springer Series in Chemical Physics*, Kodansha Scientific, Tokyo, Japan, 2005.

[11] M. I. Alonso, M. Garriga, C. A. Durante Rincon, and M. Leon, "Optical properties of chalcopyrite $CuAl_xIn_{1-x}Se_2$ alloys," *Journal of Applied Physics*, vol. 88, no. 10, pp. 5796–5801, 2000.

[12] M. I. Alonso, M. Garriga, C. A. Durante Rincón, E. Hernández, and M. León, "Optical functions of chalcopyrite $CuGa_xIn_{1-x}Se_2$ alloys," *Applied Physics A*, vol. 74, no. 5, pp. 659–664, 2002.

[13] P. Lautenschlager, M. Garriga, and M. Cardona, "Temperature dependence of the interband critical-point parameters of InP," *Physical Review B*, vol. 36, no. 9, pp. 4813–4820, 1987.

[14] D. E. Aspnes, *Handbook on Semiconductors*, vol. 2, North-Holland Publishing Company, Amsterdam, The Netherlands, 1980.

[15] M. I. Alonso, K. Wakita, J. Pascual, M. Garriga, and N. Yamamoto, "Optical functions and electronic structure of $CuInSe_2$, $CuGaSe_2$, $CuInS_2$, and $CuGaS_2$," *Physical Review B*, vol. 63, no. 7, Article ID 75203, 13 pages, 2001.

[16] R. H. Bube, *Photovoltaic Materials*, Imperial College Press, London, UK, 1998.